

COAXIAL DUMP COMBUSTOR INVESTIGATIONS

by

R. R. Craig, J. E. Drewry and F. D. Stull
Air Force Aero Propulsion Laboratory
Ramjet Technology Branch
Wright-Patterson AFB, Ohio

AE P 00 0321

An experimental investigation was conducted involving coaxial dump combustors with two different types of flameholders (annular and Y) installed at the dump station in an attempt to correlate combustor performance with previous non-reacting flowfield results. Flameholder blockage, combustor length, exit area ratio, inlet temperature, and chamber pressure were varied for both wall injection and premixed fuel conditions. Lean blowout limits, combustion efficiency, combustor total pressure drop, and wall static pressure distributions were obtained from these runs using JP-4 fuel. In addition, a limited amount of surface heating patterns and combustion oscillation data were obtained.

This work was performed under AFAPL Work Unit No. 2308S101 in 1978.

COAXIAL DUMP COMBUSTOR INVESTIGATIONS

R. R. Craig, J. E. Drewry and F. D. Stull
Air Force Aero Propulsion Laboratory
Ramjet Technology Branch
Wright-Patterson AFB, Ohio

Abstract

An experimental investigation was conducted involving coaxial dump combustors with two different types of flameholders (annular and Y) installed at the dump station in an attempt to correlate combustor performance with previous non-reacting flowfield results. Flameholder blockage, combustor length, exit area ratio, inlet temperature, and chamber pressure were varied for both wall injection and premixed fuel conditions. Lean blowout limits, combustion efficiency, combustor total pressure drop, and wall static pressure distributions were obtained from these runs using JP-4 fuel. In addition, a limited amount of surface heating patterns and combustion oscillation data were obtained.

I. Introduction

Current volume limited ramjet missile designs employ dump combustors. In this engine system, the booster rocket is integrated into the ramjet combustor to conserve missile volume. Such combustors do not contain combustor liners or conventional flameholders within the combustion region and must depend to a large extent upon recirculation zones formed by the sudden enlargement area between the inlet duct and the combustor chamber.

Several previous studies¹⁻⁴ have been conducted at the Air Force Aero Propulsion Laboratory on coaxial dump combustors. Reference 1 dealt with the scaling of small dump combustors (2" to 5" D) with a baseline dump area ratio, A_2/A_3 , of 0.25 and exhaust area ratio, A^*/A_3 , of 0.50 using both JP-4 and Shell-dyne fuel. This study showed that combustor length-to-diameter ratio, L/D , greater than 4.5 were required to obtain good combustion efficiency, η_c . Reference 2 considered the addition of flameholders to the inlet duct of the 5" D dump combustor and evaluated several basic flameholder configurations including the Y type. Increases of up to 30 counts in η_c were obtained when the best flameholder was added to the basic dump combustor with $L/D = 3$. Reference 3 extended the small scale combustor results, with and without flameholders, to a 12" D combustor and indicated that combustor performance with a flameholder does not appear to scale. The larger combustor achieved higher combustion efficiencies for equivalent flameholder blockage. Reference 4 presents basic detailed cold flowfield data and flow visualization results conducted in the Building 450 combustion research tunnel using a 3.84" D coaxial dump combustor with a dump area ratio of 0.42 and an exit area ratio of 0.42, including both Y type and annular flameholders. Gas concentration measurements of simulated fuel (argon)/air mixing were made in the combustor duct using a unique on-line, real

time gas sampling system which helped formulate a cold flowfield model.

The objective of this current effort was to extend the previous combustion studies¹⁻³ to include the baseline geometry of the cold flow study⁴ in an attempt to correlate combustor performance with non-reacting flowfield results. It was also desired to compare the symmetrical annular flameholder, which had looked promising in the cold flow study, to the basic Y type flameholder used in the previous combustion studies.

II. Experimental Procedure

Combustor Models

The combustor test hardware, as illustrated schematically in Fig. 1, was similar to the hardware used in previous test programs¹⁻³ except for actual size. It was fabricated from 6" ID stainless steel pipe and flanged at both ends. Additional length combustor sections were available which allowed for three combustor length variations of 6, 12, and 18 inches. A water cooled nozzle, 3 inches in length and with a throat diameter of 3.79 inches, was used to approximately match the $A^*/A_3 = 0.42$ ratio used in the previous cold flowfield tests.⁴

Fuel injection occurred normal to the air stream through 8 equally spaced .055" ID fixed-orifice wall injectors located 4 3/4 inches upstream of the inlet duct exit. These injectors were designed from previous fuel injection studies⁵ to provide for fuel penetration of 16 percent of the inlet diameter by the time the fuel reached the dump plane at a fuel-to-air ratio of .06 and baseline pressure conditions. Another mode of fuel injection was employed in order to simulate a premixed fuel-to-air mixture. This was done by injecting fuel into the air stream approximately 5 feet upstream of the wall injectors by means of 8 radial fingers, each having 4 spray holes. Both sets of fuel injectors had their own fuel manifold system so that tests could be conducted consecutively by merely switching a toggle switch. The inlet duct, which was 3 feet long, was fabricated from 4" ID stainless steel pipe and flanged at both ends.

Flameholder Models

The Y type flameholder was the same design as employed in Ref. 3 and is shown in Fig. 2. Three webs, consisting of strip of stainless steel bent to form an angle of 60°, were mounted from the inlet duct wall and circumferentially distributed every 120°. The base of the flameholder was in the same plane as the sudden expansion. Flameholder blockage was varied by

changing the length of the V-gutter elements. The width of the flameholder web, which was 7/8 inch, was chosen so that the flameholder would be operating well within its DeZubay stability loop for all operating conditions.

The annular wedge flameholder was the same design as employed in Ref. 4 and is also shown in Fig. 2. The annular wedge was attached to the wall by four thin rods spaced 90° apart in order to try to preserve the coaxial symmetry, rather than trying to promote interaction between the flameholder and dump region. Flameholder blockage was varied by increasing the width of the annular wedge. Nominal blockages of 25 and 35 percent were tested for both types of flameholders.

Test Rig

The combustor hardware was mounted in the Room 18 combustor thrust rig designed for measuring absolute levels of thrust. The movable deck of the thrust stand is 14 feet in length and 4 feet wide. The deck is suspended from 4 flexures 15 inches long, 4 inches wide and .036 inch thick. Static calibration of the thrust stand load cell was accomplished by applying a force at the combustor centerline through a referenced load cell. Additional calibration was accomplished prior to each combustion test as described in a following section. High pressure air was supplied from the laboratory's compressors through twelve flex hoses (2" ID) to a J-85 combustor which was modified to be used as a vitiating heater burning ethylene. Makeup oxygen was added considerably upstream of the J-85. Air flow rates were measured with flange tap, square edge orifice plates, whereas turbine type flowmeters were used for measuring fuel and oxygen flow rates to the vitiating heater and fuel flow rates to the combustor. The nozzle of the combustor model was connected to the laboratory's exhauster system by means of a flexible rolling seal, so that a choked nozzle was maintained under all combustor operating pressures. The exhaust system was maintained at approximately 3 psia.

Data Acquisition

Data was collected by means of a Mod Comp II computer controlled data acquisition system sampling at a rate of 5000 channels per second. Because of the large memory of the computer, 64K words, the computer programs were written to collect and store the raw data on magnetic disc as well as computing and displaying, on a video screen, all required facility parameters. The programs also compute and display combustor temperature based on the thrust measurement, combustion efficiency, burner pressure loss and various other parameters as the test is being conducted. Each data point is the average of 45 separate scans of the data channels in order to average out any electrical noise in the data system. At the end of each fuel-to-air ratio traverse, selected data is listed on a Tektronix 4012 graphics display terminal. After a hard copy of this data has been made, plots of combustion efficiency versus fuel-to-air ratio and pressure loss versus stream thrust parameter

are made on the graphics terminal. These are copied and the next series of test conditions established. At the end of the day, a standard computer printout is made of all the raw data and computed data.

The value of the computer system lies not only in its ability to collect and analyze large amounts of data, but also in its ability to compute rapidly certain critical parameters which tell the test engineer that all of the instrumentation is working properly. Before each test, the no air flow, pressure-area drags induced by the exhauster system are computed and compared with the thrust stand reading. If these values are within the larger of 2 lbs or 1/2%, airflow is begun. After air flow has been established, air temperature is computed from the thrust measurement and compared with the inlet air thermocouple reading. The same procedure is followed after the vitiating heater is ignited and the computed and measured temperatures must agree within ±2% before beginning the combustion tests.

Combustor Performance Calculations

The definition of combustion efficiency used throughout this paper is:

$$\eta_c = \frac{\Delta T_t}{\Delta T_{t1}}$$

where ΔT_t is the total temperature rise across the combustor as computed from the thrust measurement and ΔT_{t1} is the ideal total temperature rise for the measured fuel-to-air ratio as computed from equilibrium chemistry calculations. Since absolute thrust was measured, corrections for ambient pressure acting on the hardware and exhauster seal forces were made in order to obtain the sonic air specific stream thrust, S_a^* , see Ref. 3. A matrix of 240 values of S_a^* versus T_{t5} and P_{t5} was computed by means of equilibrium chemistry routines. These data were then input to a linear regression program to obtain a curve fit of S_a^* as a function of various combinations of T_{t5} and P_{t5} . These curve fits matched the input data within ±1% at all points. These curve fits were then used to determine T_{t5} from S_a^* and P_c .

Combustor total pressure ratios, P_{t5}/P_{t2} , are determined from measured static pressures, mass flows and thrust rather than from total pressure rakes. This method has been found to be more reliable and consistent than using total pressure probes. The combustor inlet total pressure, P_{t2} , is computed from the measured inlet static pressure, mass flow and total inlet temperature. The total pressure at the nozzle exit, P_{t5} , is computed from the throat area and the combustor total temperature as calculated from the measured thrust.

III. Discussion & Results

Baseline Combustor Tests

The 6" D baseline combustor was chosen so as to approximate the geometry of the cold flow combustor tested in the Building 450 combustor research tunnel. Table 1 shows a comparison

between the two combustors. Baseline test conditions were selected which approximated the "pressure scaling" criteria of $PD = 200$ used in the previous combustor studies.³ Two different types of flameholders, each with blockages of 25 and 35 percent, were then added to the dump plane of the baseline combustor and tested. Inlet air temperature, T_{02} , was held constant at around $1000^{\circ}R$. Fuel-to-air ratios were selected to cover the range from .025 to .06. Both modes of fuel injection, from the wall and premixed, were tested under baseline conditions. Additional runs were made at $T_{02} = 1300^{\circ}R$ for each of the flameholder configurations with wall injection only. Changes from the baseline combustor L/D were made by using shorter combustor sections resulting in lower combustion efficiencies, thereby amplifying any difference in the effectiveness of the flameholders. A matrix of the tests conducted is shown in Table 2. Combustor performance results are shown in Figs. 3 thru 9. For purposes of reference, it should be noted that the value of fuel-to-air ratio, f/a , corresponding to an equivalence ratio of 1 is .0677.

The combustor performance data shown in Fig. 3 was obtained for the baseline test geometry without flameholders. The significant influence of combustor length and fuel injection mode on combustion efficiency is apparent from these results. It should be mentioned that, for the test conditions at $L/D = 1$ with wall fuel injection, the ramburner would not sustain combustion.

The results shown in Figs. 4 and 5 are the parametric performance data for the baseline test geometry with flameholders. In Fig. 4 combustion efficiency is given as a function of combustor L/D and fuel injection mode for tests with the Y type flameholders at inlet air total temperatures of $1000^{\circ}R$ and $1300^{\circ}R$. Similar results which were obtained for the baseline test geometry with the annular wedge flameholders are shown in Fig. 5. The overall influence of the various flameholders on combustor performance relative to that without any flameholder is obvious when comparing the results of Figs. 4 and 5 to those in Fig. 3. In the case of the Y type flameholder, the highest combustion efficiency was always obtained at the lowest fuel-to-air ratio, with an almost linear decrease in η_c occurring with increased f/a . Ramburner operation at $L/D = 1$ was possible with the Y type flameholder installed. However, as can be seen in Fig. 4, the performance for this case was not very good.

The performance results obtained using the annular wedge flameholders were markedly different from those obtained with the Y type devices, particularly at $L/D = 1$. Ramburner combustion efficiency, as a function of f/a , did not follow the same consistent trend observed with the Y type flameholders. In the tests with the annular flameholders, the total temperature of the inlet air had a more significant influence on combustor performance than was apparent with the other test configurations. The best overall ramburner combustion efficiencies for all test configurations were obtained using the annular flameholders

with $L/D = 3$ and $T_{02} = 1300^{\circ}R$. It also should be noted that at $L/D = 3$, the variation of η_c with f/a was very slight over the full range of ramburner operation with the annular flameholders installed. At the shorter combustor lengths of 6 and 12 inches (L/D equal to 1 and 2, respectively), the performance pattern became more erratic in nature, as demonstrated in Fig. 5 by the sudden changes in combustion efficiency during the f/a excursion. Highly oscillatory combustion was observed during some periods of operation. This phenomena will be discussed further in a later section.

In Figs. 6-8, comparative plots of ramburner performance results for the various test configurations are shown for each combustor L/D at $T_{02} = 1000^{\circ}R$ and $1300^{\circ}R$. In terms of flameholder geometry, the observed performance is inconclusive. Under some test conditions the annular wedge appears superior, while under others it is obviously inferior.

Chamber Pressure And Exit Area Ratio

Combustor pressure was decreased from baseline conditions by decreasing the air mass flow through the combustor by 50 percent. These results are shown in Fig. 9 for the 0.25-Y and 0.25-AW flameholder combustors, resulting in measured chamber pressures of 15 to 16 psia and 14 to 15 psia respectively. Under these conditions, the baseline combustor without a flameholder could not sustain combustion. When air mass flow was again decreased by 50 percent, corresponding to $PD = 50$, none of the combustor configurations could sustain combustion. Figure 9 shows a significant decrease in η_c as chamber pressure is decreased for both types of flameholders. Previous results with a 12" D combustor showed small differences in combustion efficiency when chamber pressure was reduced from 16 to 10 psia, thereby indicating that it is not the absolute pressure level in the combustor that is the controlling parameter, but rather pressure times diameter (PD).

The effect of increasing nozzle throat diameter, D^* , from 3.79 inches to 4.25 inches produced no appreciable change in performance for the 0.25-Y flameholder. However, in the case of the 0.25-AW flameholder, a significant increase in performance was measured with the larger D^* . The reason for the sudden decrease in η_c at the highest value of f/a for this test condition is not presently clear.

Other Factors

In addition to the above parametric combustor tests, a few exploratory tests were conducted on other variations. In order to assure that hysteresis effects were not prevalent during a combustor run over a full fuel-to-air ratio excursion, two separate runs were conducted on the baseline configurations (no FH, 0.25-Y and 0.25-AW) with fuel-to-air ratio increasing in one run, and fuel-to-air ratio decreasing in the second run. Less than a 2 to 3 count change in combustion efficiency was noted for all test cases. Subsequently, for the rest of the test program only one run was conducted. It was

decided to use a decreasing fuel-to-air ratio in order to avoid a cold combustor wall temperature near the lean-blow out limits, where wall temperature effects were expected to be the greatest.

Likewise, a few variations in inlet diameter, D_2 , were run with the baseline 0.25-Y flameholder combustor to observe the effects of dump area ratio. Performance was increased about 10 counts over most of the f/a range covered when the baseline A_2/A_3 was decreased from 0.44 to 0.35. Decreasing A_2/A_3 still further to 0.25 resulted in a slight combustion efficiency improvement, but only over the middle f/a range. This trend is in agreement with previous small scale combustor tests ($D_3 \leq 6''$), but is contrary to results obtained with larger scale combustor tests ($D_3 = 12''$). Apparently, the dump area ratio for optimum performance does not follow "PD scaling criteria."

The lean blow-out data was in general agreement with the previous combustor studies, occurring at $f/a \leq .015$ for the wall injection mode and at $f/a \sim .044$ for the premixed mode (slightly higher than $f/a \sim .035$ reported in Ref. 2). The addition of flameholders did not appear to change the lean blow-out limit, but did introduce considerably more scatter ($.040 \leq f/a \leq .048$) into the data for the premixed mode.

Combustor Pressure Losses

Combustor total pressure losses were not measured directly with a total pressure rake because of the difficulty in obtaining a representative mass averaged total pressure in a reacting combustor with unsteady flow and large recirculation zones. Only when the combustor is very long so that the flow has time to reattach itself to the wall and become established, can reasonable pressure measurements be made with a water-cooled pressure rake. Instead, combustor pressure recovery, P_{T5}/P_{T2} , was determined from measured inlet static pressure, mass flow, and thrust as described in Section II.

Figure 10 shows these results for the baseline combustors at 1300°R plotted against the heat addition parameter, $S_a^*/\sqrt{T_{02}}$, which is the sonic stream thrust divided by the square root of inlet total temperature. For a constant area combustor, pressure recovery will decrease as heat addition increases. However, for the dump combustor, pressure losses are a combination of aerodynamic losses, including the sudden expansion loss, plus heat addition losses. As heat addition increases, inlet Mach number decreases and the reduced aerodynamic losses overshadow the increased heat addition losses; hence, combustor pressure recovery increases. This is evident in Fig. 10 with the largest flameholder blockages (35%) having the steepest slope due to larger aerodynamic losses. For the baseline combustor without flameholder, the aerodynamic losses were only slightly greater than the heat addition losses, hence these losses tend to cancel each other and pressure recovery remains relatively constant over the range of fuel-to-air ratios tested. The data points on the far left hand side were obtained prior to combustion. Virtually no difference in

pressure recovery was noted between the 25% blockage Y and annular flameholders. The 35% blockage annular flameholder showed a slightly greater pressure loss than did the 35% blockage Y flameholder.

Static Pressure Distributions

The baseline combustor ($L/D = 3$) contained wall static pressure taps every inch downstream of the dump plane. Data was recorded from each pressure transducer prior to a combustion run and during selected fuel-to-air ratios. A comparison of the baseline combustor with no flameholder and no combustion ($f/a = 0$) is made with similar cold flow test data from Ref. 4 and is shown in Fig. 11 as an axial static wall pressure distribution normalized by dump step height, h , where $h = (D_3 - D_2)/2$. Although a slight difference in the absolute values are seen in the region near the dump, the characteristic shape of the curves are similar. This difference is attributed, in part, to the location where the inlet total pressure, P_{T2} , was measured in both experiments. The wall pressure plotted at $x/D = 0$ in the present tests was actually the inlet static pressure measured upstream of the wall fuel injectors and the flameholder. Also noted in this figure is the reattachment point, indicated by the dashed line L'/h , as determined from flow visualization techniques in the cold flow equipment.

Figures 12 thru 14 show the axial static wall pressure distributions normalized by combustor diameter, D_2 , for the baseline combustors at $T_{02} = 1300^\circ\text{R}$ for various fuel-to-air ratios, and are representative of the vast amount of static pressure data obtained. It is noted that without combustion ($f/a = 0$) the axial static wall pressure distributions characterize the type of flameholder employed and are very consistent and well defined. This is not true once combustion had occurred, as various patterns were observed. In some cases wall static pressure increased with distance downstream of the dump, and in other cases it decreased with length. In some cases the static pressure distribution was not appreciably affected by fuel-to-air ratio, and in others it was a strong function of fuel-to-air ratio. This is dramatically illustrated by the 25% annular flameholder in Fig. 14 where the only difference in test conditions was the inlet air temperature. The only general observation that could be made after looking at all of the wall static pressure data and the corresponding combustion efficiency curves was that very high combustion efficiencies tended to cause a decrease in wall static pressure with length, whereas poor combustion efficiencies tended to show an increase in wall static pressure with length. Likewise, when combustion efficiency was relatively constant over an entire f/a range, the wall static distribution tended not to show a large variation with f/a ; however, this was not always true as exceptions were noted. Attempts to correlate a given axial wall static pressure to combustion efficiency were not too successful, as many apparent inconsistencies were noted. As an example, combustion efficiencies are tabulated in Table 3 corresponding to the fuel-to-air ratios shown in Figs. 12 thru 14.

From the above, it can be seen that caution must be exercised in attempting to define combustor performance from its static pressure distribution alone. This can have severe implications in attempting to design a ramjet control system based solely on a wall static pressure measurement, unless the combustor has been well characterized.

Surface Heating Patterns

Using bare wall stainless steel combustor models instead of water-cooled combustors allows one to obtain additional information in regards to what is happening within the combustor, and how the fuel injector/flameholder assembly is behaving. This is shown in Fig. 15 where photographs were taken of the hot combustor as viewed from the control room TV screen. Figure 15a shows the surface heating pattern for the 0.25-Y flameholder taken under the same test conditions as for the pressure distribution data previously shown in Fig. 13. Large circumferential temperature gradients are noted near the dump end of the combustor due to the unsymmetrical pattern of the Y flameholder. Surface temperature in the lightest regions, corresponding to wake regions from the flameholder struts, approached 1500°F as determined from other test programs in which thermocouples had been attached to the combustor wall. When uniform fuel injection was employed, the surface heating pattern became somewhat more uniform, although variations caused by the wake of the three flameholder struts could still be observed. One of the virtues in observing surface heating patterns is that it tells where to locate thermocouples in order to obtain the maximum amount of quantitative heat transfer data with a limited number of thermocouples. This is especially valuable in relating to ramburner thermal protection investigations.

Figure 15b shows that a more uniform heating pattern is obtained with the 25% annular flameholder, although some circumferential variations are seen which correspond to the location of the four support struts which held the annular wedge in place.

Combustor Pressure Oscillations

During many of the combustion runs, an audible screech could be heard over a portion of the f/a range. A close coupled, high frequency response Kistler pressure transducer was attached to the front combustor flange to detect any unusually large pressure oscillations occurring. Output of the transducer was connected to a Tektronix oscilloscope to determine the amplitude of the pressure fluctuations and then to a fast Fourier transform spectral analyzer to determine the dominant frequencies. In general, two distinct types of oscillation were detected during the test series: (1) a low frequency oscillation on the order of 200 Hz with peak to peak amplitudes as high as 100% of the average chamber pressure, and (2) high frequency oscillations between 2500 and 5000 Hz with peak to peak pressure fluctuations as much as 50 percent of the average chamber pressure. It was these latter frequencies which could be heard as

combustor screech during some of the runs. Figure 16 shows examples of these types of oscillations detected while running the 25% annular flameholder under similar flow conditions at inlet air temperatures of 1000°R. Figure 16a is for the baseline ($L/D = 3$) combustor whereas Fig. 16b is for the short ($L/D = 1$) combustor. The change in combustor length alone was responsible for changing the pressure oscillations from the low frequencies to the high frequency screech. This may help to explain the peculiar nature of some of the combustion efficiency data noted earlier for the short combustor with the annular flameholder. Although the low frequency oscillations do not seem to have any significant effect on combustion efficiency, the high frequency oscillations can have a significant effect in increasing combustor efficiency by drastically altering the combustor flowfield. This effect was noted in a previous in-house combustor experiment in which high speed movies were taken of a 6 inch quartz dump combustor ($A_2/A_3 = 0.25$) in an attempt to observe the nature of the reacting flowfield. As the f/a was increased from .035 to .04 a drastic change in the entire flame pattern was observed and at the same time combustor screech was heard with subsequent breakage of the quartz chamber. Unfortunately, high frequency instrumentation was not used during that experiment, hence the combustor oscillations at that instant were not recorded. The high speed movies also illustrated the unsteadiness of the flame fronts both with and without high frequency combustor oscillations.

Some naive attempts were made to characterize the present oscillations as longitudinal, transverse, or radial waves based on the fundamental frequencies associated with a closed cylindrical vessel. These attempts were unsuccessful. For the low frequency instabilities, it was assumed that the sonic nozzle was one of the reflecting surfaces. The distance to the other reflecting surface was then computed assuming the measured frequency was the first harmonic. The required distance turned out to be midway in the inlet duct and thus incompatible with the requirements for a reflecting surface. The low frequency oscillations seem to be associated with the shedding of a ring vortex off the surface of the inlet duct at the dump station of the combustor. This frequency seemed to be independent of whether or not there was a flameholder in the inlet duct. In fact, using the Strouhal number of 0.21 for cylinders with a body diameter of 6 inches yields frequencies remarkably close to the measured values. However, in the absence of combustion, one would also expect to find some shedding frequency. Although the nonburning pressure oscillations were only 3 percent of the average chamber pressure, there was a measurable, predominant frequency which turned out to be 2 1/2 times the calculated shedding frequency.

The high frequency screech of the annular flameholder, at times, was also of the same frequency as predicted for vortex shedding off its base region. However, the oscillations can be just as easily identified as the first tangential, first radial, or second tangential modes of oscillation depending on what one assumes for the effective speed of sound for the chamber.

Correlation to Cold Flow Results

As previously mentioned, a comprehensive series of cold flow dump combustor tests was conducted prior to the present effort. A direct correlation of cold flow mixing results with then available ramburner performance data was made in Ref. 4. The ramburner test results now being reported provide a more extensive and consistent set of data with which to correlate. In Ref. 4 a comparison between centerline concentration of simulated injected fuel and ramburner combustion efficiency was given as a function of combustor L/D for various test configurations. It was shown that the cold flow mixing results did, in fact, correlate quite well in terms of overall combustor performance for mixing-limited configurations.

Using the same basis of comparison as given in Ref. 4, it is possible to make predictions of ramburner performance via cold flow mixing data for each of the configurations tested in this effort. These performance estimates, along with the actual measured combustor performance data, are given in Table 4. The ramburner performance results are those obtained at $f/a \sim .045$ which was being simulated in the cold flow tests. As can be seen in Table 4 some of the performance predictions agree quite well with observed performance, while in other cases the agreement is not so good. One trend is clearly obvious; namely, that better overall agreement is obtained at the higher inlet air total temperature of 1300°R than at the lower value of 1000°R. This would seem to indicate that improved vaporization of the liquid JP-4 was occurring at the higher total temperature, thus resulting in a better simulation with respect to the wall injection and mixing of a gaseous fuel with cold flow air.

The performance correlations given in Table 4 certainly do not tell the complete story. For that one must look at results over the entire range of f/a . The onset of highly oscillatory combustion at some point in a given f/a excursion, which results in large increases in η_c is certainly not predictable on the basis of cold flow results.

IV. Conclusions

The performance characteristics of the two types of flameholders were very different, with the Y type flameholders showing consistent trends of decreasing combustion efficiency with increasing f/a . On the other hand, the annular flameholder showed less sensitivity to f/a and L/D but a much greater dependency upon inlet air temperature. This suggests that a more effective flameholder could be designed by combining features of both types of flameholders; i.e., replacing the thin support rods of the annular wedge with the V-gutter webs of the Y type so as to promote interaction between the annular wedge and the dump region.

Conducting premixed and wall injection tests consecutively can provide some insight into the sensitivity of fuel penetration, atomization and vaporization effects on combustor performance. Such tests help to define the potential gains to be made by fine tuning the fuel injector assembly with a given flameholder configuration.

The use of wall static pressure distributions as the sole basis for predicting overall combustor behavior is not felt to be sufficient without additional supporting data.

Surface heating patterns, obtained by using bare wall combustors, can be of value in developing ramburner thermal protection systems. The patterns may also be useful in locating reattachment points if, for combusting flows, the point of maximum heat transfer corresponds to the flow reattachment point.

Adequate high frequency pressure instrumentation is essential for detecting the occurrence of combustor oscillations which can affect combustor performance and durability. Combustor screech has profound effects on combustor performance, but can also produce very high local heating rates which can be detrimental to the combustor chamber thermal protection system. Low frequency oscillations appear to have little influence on combustor performance or heating patterns, but could impact inlet stability margins.

Detailed cold flow mixing results are useful in designing combustors. If the fuel-air distribution is not well mixed at the exit of the combustor, there is no chance that the combustor will perform well. The converse, however, is not true. Actual combustor performance is strongly dependent on many additional variables.

References

1. Stull, F. D., Craig, R. R., and Hojnacki, J. T., "Dump Combustor Parametric Investigations," ASME Fluid Mechanics of Combustion, Joint Fluids Engineering and CSME Conference, Montreal, Quebec, May 13-15, 1974.
2. Stull, F. D. and Craig, R. R., "Investigation of Dump Combustors with Flameholders," AIAA Paper 75-165, AIAA 13th Aerospace Sciences Meeting, Pasadena, California, January 20-22, 1975.
3. Craig, R. R., Buckley, P. L., and Stull, F. D., "Large Scale Low Pressure Dump Combustor Performance," AIAA Paper 75-1303, AIAA/SAE 11th Propulsion Conference, Anaheim, California, September 29 - October 1, 1975.
4. Drewry, J. E., "Fluid Dynamic Characterization of Sudden-Expansion Ramjet Combustor Flowfields," AIAA Journal, Vol. 16, April 1978, pp. 313-319.
5. Hojnacki, J. T., "Ramjet Engine Fuel Injection Studies," AFAPL-TR-72-76, August 1972.

Table 1 Comparison of test models

	Cold Flow Model	Baseline Combustor
D ₂ (in)	2.50	4.00
D ₃ (in)	3.84	6.00
D* (in)	2.50	3.79
L _C (in)	15.1	18.0
L _N (in)	1.5	3.0
h (in)	0.67	1.0
Injector Orifice Diameter (in)	0.035	0.055
Dist. from Inj. to Dump (in)	2.5	4.75
L _C /D ₃	3.93	3.00
L _{C+N} /D ₃	4.32	3.50
Λ ₂ /Λ ₃	0.42	0.44
A*/A ₃	0.42	0.40
M _{inlet}	0.70	0.54

Table 3 Tabulation of combustion efficiency

No Flameholder T ₀₂ = 1300°R		0.25-Y 1300°R		0.25-AW 1000°R		0.25-AW 1300°R	
Fig 12		Fig 13		Fig 14a		Fig 14b	
f/a	η _c	f/a	η _c	f/a	η _c	f/a	η _c
.031	.687	.027	.883	.026	.712	.026	.773
.041	.717	.037	.863	.061	.724	.041	.883
.060	.663	.045	.814			.058	.901
		.059	.754				

Table 4 Baseline combustor correlation of performance data at f/a = 0.045

Configuration	L/D	Cold Flow Mixing Predictions		Ramburner Performance	
		η _c /η _{cmax}	η _c	η _{c1000}	η _{c1300}
No FH	3	0.90	0.81	0.58	0.70
	2	0.50	0.45	0.48	0.60
	1	0.00	0.00	--	--
0.25-Y	3	0.95	0.85	0.75	0.80
	2	0.85	0.76	0.62	0.75
	1	0.30	0.27	0.25	0.39
0.25-AW	3	1.00	0.90	0.73	0.89
	2	0.98	0.88	0.75	0.90
	1	0.55	0.49	0.55	0.80

Table 2 Matrix of test points

Flameholder →		None		0.25-Y		0.25-AW		0.35-Y		0.35-AW		A*/A ₃	W _{air} (lb/sec)
L/D	T ₀₂ →	1000	1300	1000	1300	1000	1300	1000	1300	1000	1300		
3	Wall Inj. Premix	X	X	X	X	X	X	X	X	X	X	0.40	3.2
		X		X		X		X		X			
2	Wall Inj. Premix	X	X	X	X	X	X	X	X	X	X	0.40	3.2
		X		*		*		X		X			
1	Wall Inj. Premix	*	*	X	X	X	X	X	X	X	X	0.50	3.2
		X		X		X		X		X			
3	Wall Inj. Premix	X	X	X	X	X	X					0.50	3.2
		X		X		X							
3	Wall Inj. Premix	*		X		X						0.40	1.6

* Would not sustain combustion.

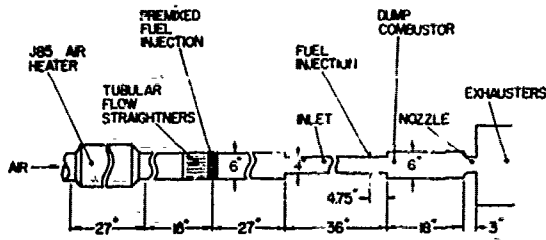
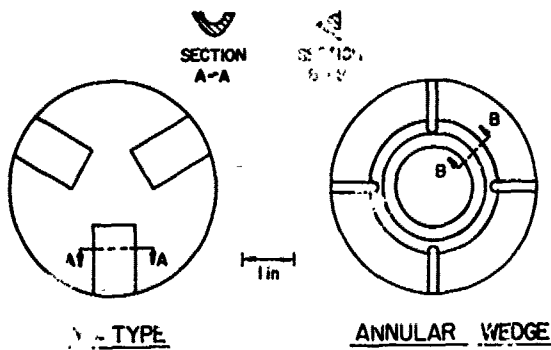


Fig. 1 Schematic illustration of AFAPL combustor thrust rig.



Y-TYPE

ANNULAR WEDGE

Fig. 2 Flameholder configurations.

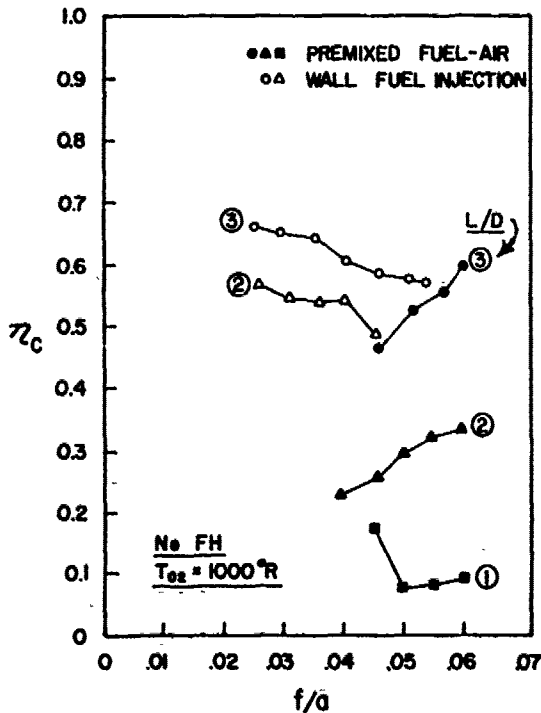
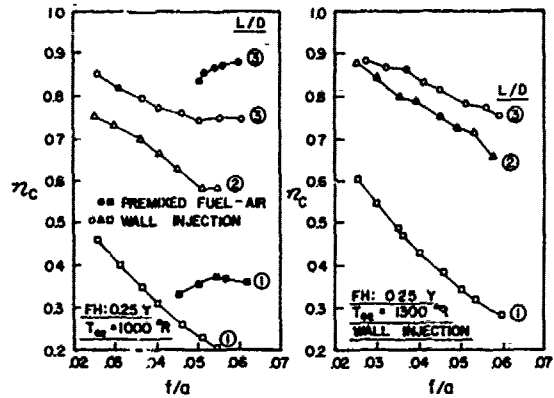
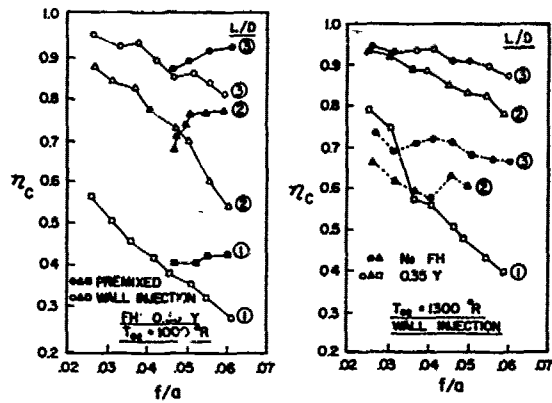


Fig. 3 Baseline combustor performance without flameholders.

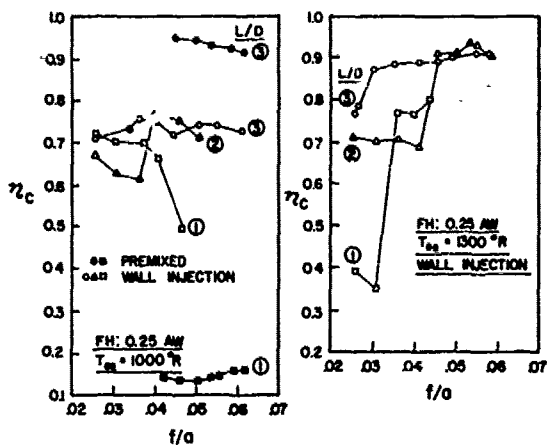


a. 25% blockage.

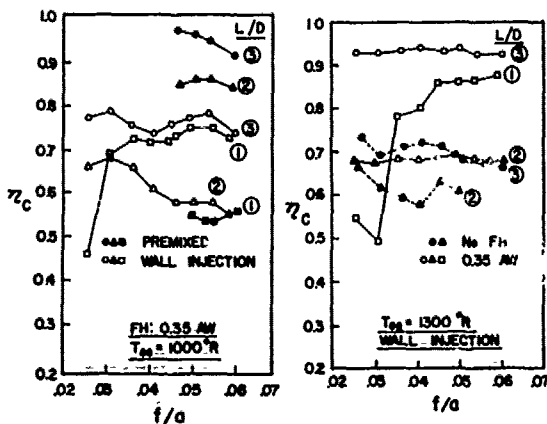


b. 35% blockage.

Fig. 4 Baseline combustor performance with Y type flameholders.



a. 25% blockage.



b. 35% blockage.

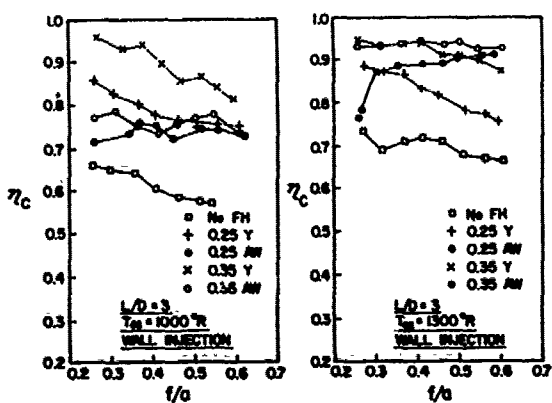


Fig. 6 Ramburner performance for various test configurations at $L/D = 3$.

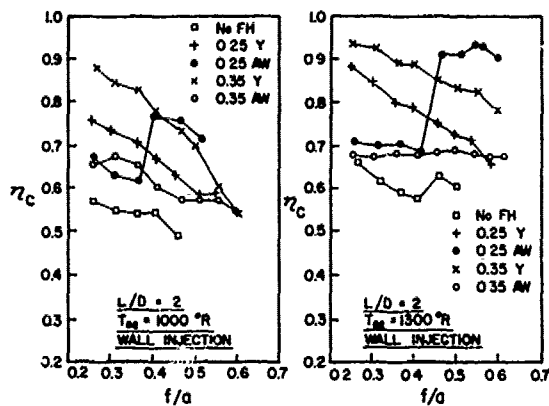


Fig. 7 Ramburner performance for various test configurations at $L/D = 2$.

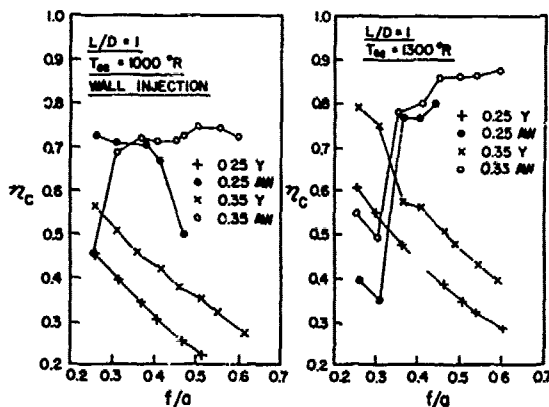


Fig. 8 Ramburner performance for various test configurations at $L/D = 1$.

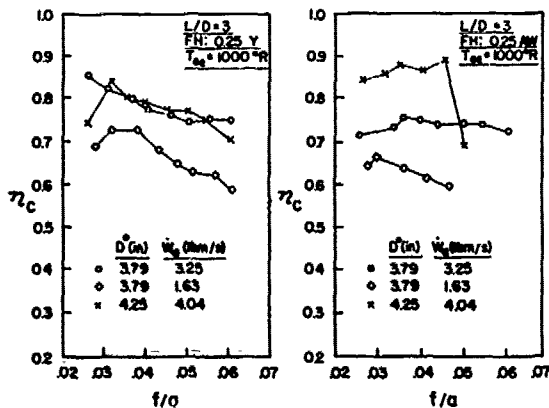


Fig. 9 Combustor performance for decreased W_A and increased D^* .

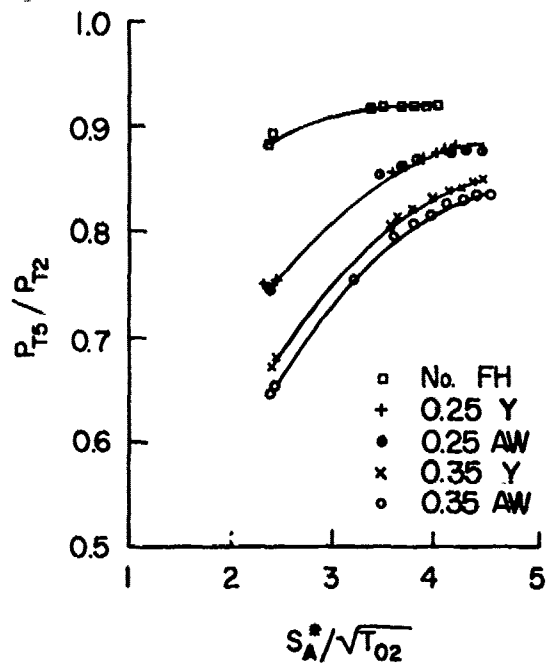


Fig. 10 Baseline combustor pressure loss.

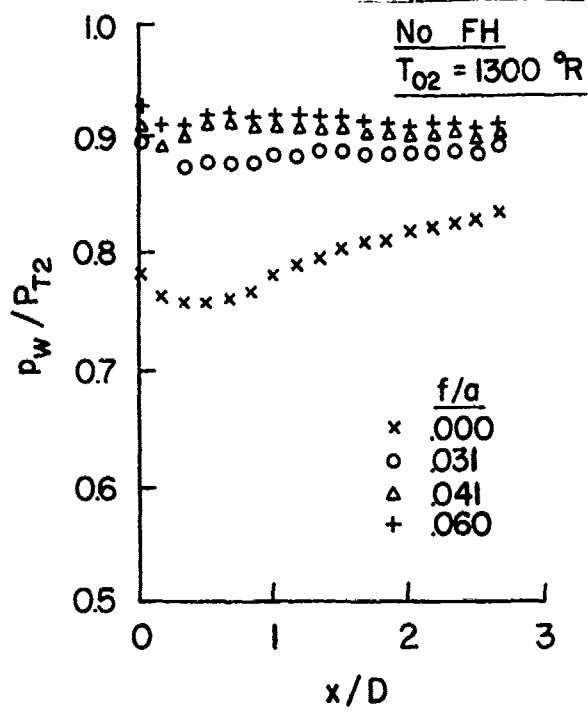


Fig. 12 Baseline combustor wall pressure distribution without flameholders.

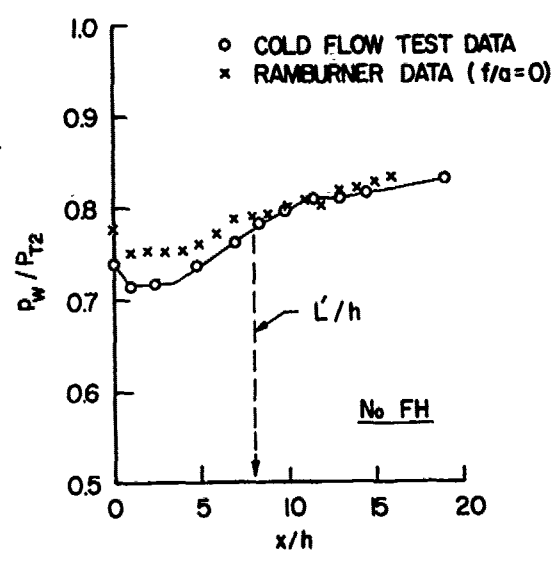


Fig. 11 Comparison of cold flow wall pressure distribution.

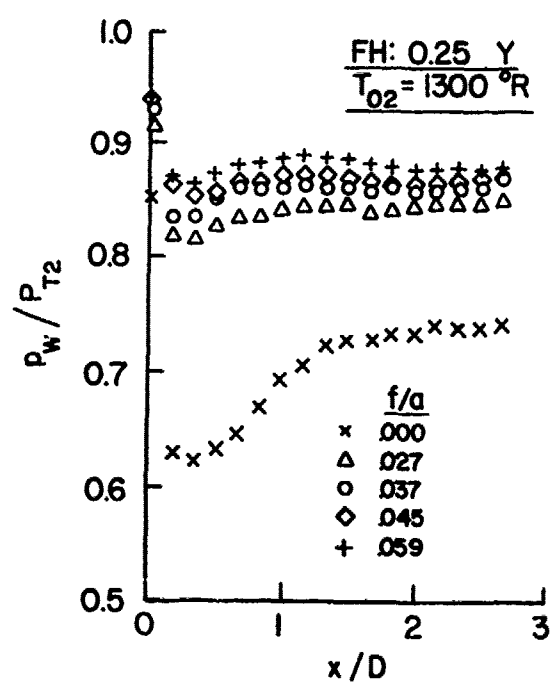


Fig. 13 Baseline combustor wall pressure distribution with Y type flameholders.

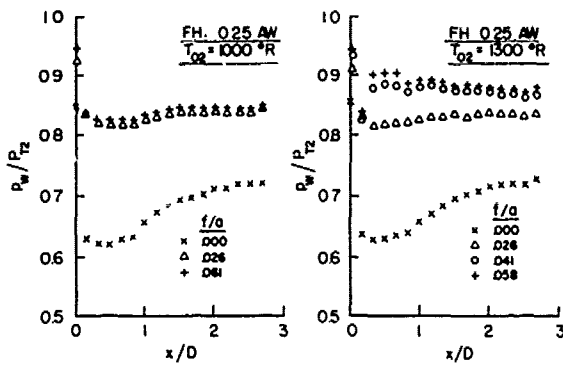
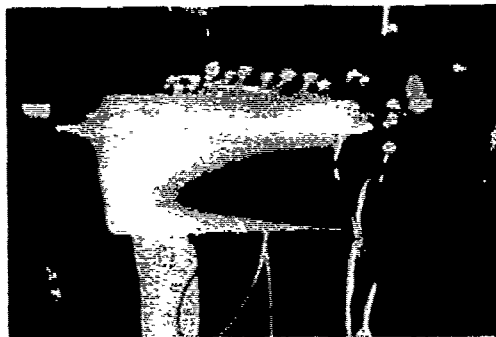
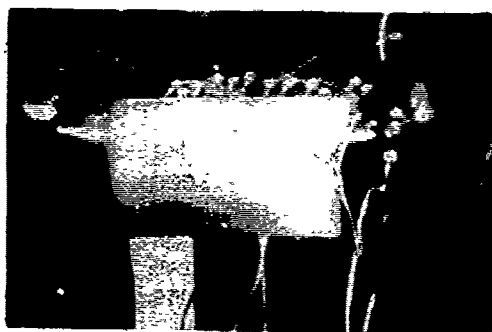


Fig. 14 Baseline combustor wall pressure distribution with annular wedge flameholders.

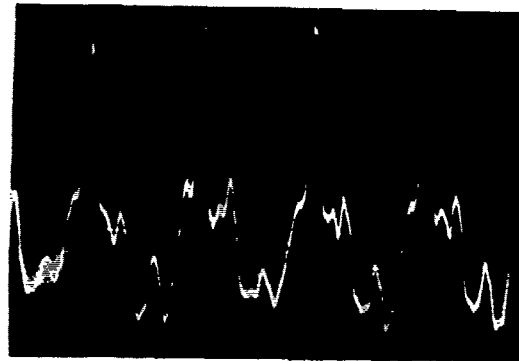


a. 0.25-Y flameholder.

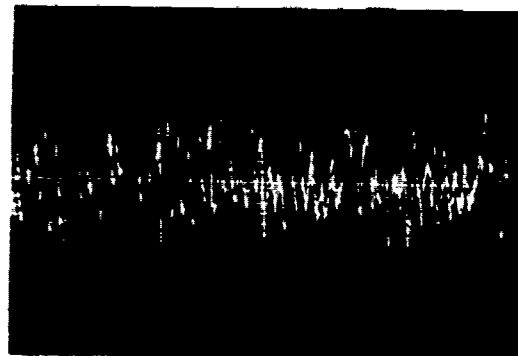


b. 0.25-AW flameholder.

Fig. 15 Surface heating patterns for baseline combustor.



a. $L/D = 3$: 5 psi/cm and 2 millisecc/cm



b. $L/D = 1$: 5 psi/cm and 1 millisecc/cm

Fig. 16 Combustor pressure oscillations for 0.25-AW flameholder.

